

Combined radiation and natural convection in a vertical conical annular porous medium

D. Prabhakar¹, S. Ravikumar² and R. Siva Prasad³

¹*fire office, Guntakal, Anantapur, Andhra Pradesh, India.*

²*Department of Mathematics, N.B.K.R. Institute of Science and Technology, Vidyannagar, SPSR Nellore, Andhra Pradesh-515401, India.*

³*Department of Mathematics, Sri Krishna Devaraya University, Anantapur, Andhra Pradesh, India.*

ABSTRACT

In this paper, we concentrate on the study of heat transfer by natural convection in a saturated porous medium including Radiation confined in a vertical conical annular porous medium. In this study, Finite Element Method (FEM) has been used to solve the governing partial differential equations. Results are presented in terms of average Nusselt number (\overline{Nu}), streamlines and Isothermal lines for various values of Rayleigh number (Ra), Cone angle (C_A) Radius ratio (R_r) and Radiation parameter (R_d).

Keywords: Vertical conical annular porous medium, Natural convection, Streamlines and Isothermal Cone angle, Radius ratio, Radiation parameter.

INTRODUCTION

Study of buoyancy – induced convection flow and heat transfer in fluid – saturated porous medium has recently attracted considerable interest because of a number of important energy – related engineering and geophysical applications such as thermal insulation of buildings, geothermal engineering, and enhanced recovery of petroleum resources, filtration processes, ground water pollution and sensible heat storage beds.

Free convection about a vertical flat plate embedded in a porous medium at high Rayleigh numbers was analyzed by Cheng and Minkowycz [1]. Na and Pop [2] studied free convection flow past a vertical flat plate maintained at a nonuniform surface temperature embedded in a saturated porous medium and presented numerical results by employing a two-point finite difference method. [3] studied the free convection from a vertical plate embedded in saturated porous mediums.

In the aspect of vertical cylinder, Minkowycz and Cheng [4] were the first authors to present free convection about vertical cylinder embedded in a porous medium. Yücel [5] employed an implicit finite difference method to examine the free convection about a vertical cylinder in a porous medium. [6] used finite difference method and improved perturbation solution for free convection on a vertical cylinder embedded in a saturated porous medium.

Merkin [7] investigated the free convection from an isothermal vertical cylinder in a saturated porous medium. Bassom and Rees [8] extended the work of Merkin [7] to investigate the variable wall temperature case. The governing equations are also solved numerically using the Keller box method. The natural convection, the existence of the temperature difference between the surface and the ambient causes the radiation effect may become important. Hossain and pop [9] investigated the effect of radiation on Darcy's buoyancy induced flow along an in

dined surface placed in porous media employing the implicit finite difference method together with Keller box elimination technique. Steady two – dimensional natural convection flow through a porous medium bounded by a vertical infinite porous plate in the presence of radiation is considered by Raptis [10].

Heat transfer by mixed convection in laminar boundary-layer flow has been analyzed extensively for flat plate geometry in saturated porous media in vertical, horizontal, and inclined orientations. Typical studies can be found, for example, in [11-14]. On the other hand, heat transfer by simultaneous natural convection and thermal radiation has not received as much attention. This is unfortunate because thermal radiation will play a significant role in the overall surface heat transfer in situations where convection heat transfer coefficients are small, as is the case of natural convection. Viskanta and Gresh [15] considered the effects of thermal radiation on the temperature distribution and the heat transfer in an absorbing and emitting media over a wedge by using the Rosseland diffusion approximation. Natural convection radiation over horizontal surfaces was presented by Ali et al. [16]. Bakier and Gorla [17] considered the effect of thermal radiation on the mixed convection from horizontal surfaces in saturated porous media. Hassain and Ress [18] investigated the natural convection, radiation interaction on boundary layer along an isothermal plate inclined at a small angle to the horizontal. Recently A.Y. Bakier [19] investigated the thermal radiation effect on mixed convection from vertical surfaces in saturated porous media. Srinadh et al [20] investigated the MHD Free convection flow of couple stress fluid in a vertical porous layer. Gorla and Zinalabedini. J. Girish kumar et al [21] investigated the Mass transfer effects on MHD flows exponentially accelerated isothermal vertical plate in the presence of chemical reaction through porous media. K.Chand et al [22] investigated the Hydromagnetic oscillatory flow through a porous medium bounded by two vertical porous plates with heat source and solet effect. . Kumari et al. Jyoti prakash et al [23] investigated the A mathematical theorem in magnetothermohaline convection in porous medium. Sravan N. Gaikwad [24] investigated the The effect of Solet parameter on the onset of double diffusive convection in a Darcy porous medium saturated with couple stress fluid.

2 FORMULATION OF THE PROBLEM

A vertical annular cone of inner radius r_i and outer radius r_o as depicted by schematic diagram as shown in figure (A) is considered to investigate the heat transfer behavior. The co-ordinate system is chosen such that the r-axis points towards the width and z-axis towards the height of the cone respectively. Because of the annular nature, two important parameters emerge which are Cone angle (C_A) and Radius ratio (R_r) of the annulus. They are defined as

$$C_A = \frac{H_t}{r_o - r_i}, \quad R_r = \frac{r_o - r_i}{r_i}$$

where H_t is the height of the cone.

The inner surface of the cone is maintained at isothermal temperature T_h and outer surface is at ambient temperature T_∞ . It may be noted that, due to axisymmetry, a section of the annulus is sufficient for analysis purpose.

We assume that the flow inside the porous medium is assumed to obey Darcy law and there is no phase change of fluid. The properties of the fluid and porous medium are homogeneous, isotropic and constant except for variation of fluid density with temperature. The fluid and porous medium are in thermal equilibrium.

Continuity equation:

$$\frac{\partial(ru)}{\partial r} + \frac{\partial(rw)}{\partial z} = 0 \quad (2.2.1)$$

The velocity in r and z directions can be described by Darcy law as velocity in horizontal direction

$$u = \frac{-K}{\mu} \frac{\partial p}{\partial r} \quad (2.2.2)$$

velocity in vertical direction

$$w = \frac{-K}{\mu} \left(\frac{\partial p}{\partial z} + \rho g \right) \quad (2.2.3)$$

the permeability K of porous medium can be expressed as

$$K = \frac{D_p^2 \phi^3}{180(1 - \phi)^2} \quad (2.2.4)$$

The variation of density with respect to temperature can be described by Boussinesq approximation as

$$\rho = \rho_{\infty} [1 - \beta_T (T - T_{\infty})] \quad (2.2.5)$$

Momentum Equation :

$$\frac{\partial w}{\partial r} - \frac{\partial u}{\partial z} = \frac{gK\beta}{\nu} \frac{\partial T}{\partial r} \quad (2.2.6)$$

Energy equation

$$u \frac{\partial T}{\partial r} + w \frac{\partial T}{\partial z} = \alpha \left(\frac{1}{r} \frac{\partial}{\partial r} \left(r \frac{\partial T}{\partial r} \right) + \frac{\partial^2 T}{\partial z^2} \right) - \frac{1}{\rho C_p} \frac{1}{r} \frac{\partial}{\partial r} (r q_r) \quad (2.2.7)$$

The last term in the right hand side of the equation (2.2.7) represents radiation effect.

The continuity equation (2.2.1) can be satisfied by introducing the stream function ψ as

$$u = -\frac{1}{r} \frac{\partial \psi}{\partial z} \quad (2.2.8)$$

$$w = \frac{1}{r} \frac{\partial \psi}{\partial r} \quad (2.2.9)$$

Rosseland approximation for radiation is

$$q_r = \frac{4n^2 \sigma}{3\beta_R} \frac{\partial T^4}{\partial r} \quad (2.2.10)$$

The corresponding dimensional boundary conditions are

$$\text{at } r = r_i, \quad T = T_w, \quad \psi = 0 \quad (2.2.11a)$$

$$\text{at } r = r_0, \quad T = T_{\infty}, \quad \psi = 0 \quad (2.2.11b)$$

(except at $z = 0$)

The new parameters arising due to cylindrical co-ordinates system are

$$\text{Non-dimensional Radius} \quad \bar{r} = \frac{r}{L} \quad (2.2.12a)$$

$$\text{Non-dimensional Height} \quad \bar{z} = \frac{z}{L} \quad (2.2.12b)$$

$$\text{Non-dimensional stream function} \quad \bar{\psi} = \frac{\psi}{\alpha L} \quad (2.2.12c)$$

$$\text{Non-dimensional Temperature} \quad \bar{T} = \frac{(T - T_{\infty})}{(T_w - T_{\infty})} \quad (2.2.12d)$$

$$\text{Rayleigh number} \quad Ra = \frac{g\beta_T \Delta T K L}{\nu \alpha} \quad (2.2.12e)$$

$$\text{Radiation parameter} \quad R_d = \frac{4\sigma n^2 T_c^3}{\beta_R K_s} \quad (2.2.12f)$$

The non-dimensional equations for the heat transfer in vertical cone are

Momentum equation:

$$\frac{\partial^2 \bar{\psi}}{\partial \bar{z}^2} + \bar{r} \left(\frac{1}{\bar{r}} \frac{\partial \bar{\psi}}{\partial \bar{r}} \right) = \bar{r} Ra \frac{\partial \bar{T}}{\partial \bar{r}} \quad (2.2.13)$$

Energy equation :

$$\frac{1}{r} \left[\frac{\partial \bar{\psi}}{\partial r} \frac{\partial \bar{T}}{\partial z} - \frac{\partial \bar{\psi}}{\partial z} \frac{\partial \bar{T}}{\partial r} \right] = \left(\frac{1}{r} \frac{\partial}{\partial r} \left(\left(1 + \frac{4R_d}{3} \right) r \frac{\partial \bar{T}}{\partial r} \right) + \frac{\partial^2 \bar{T}}{\partial z^2} \right) \quad (2.2.14)$$

The corresponding non-dimensional boundary conditions are

$$\text{at } \bar{r} = \bar{r}_i, \bar{T}=1, \bar{\psi} = 0 \quad (2.2.15)$$

3 SOLUTION OF THE PROBLEM

Applying Galerkin method to momentum equation (2.2.13) yields:

$$\{R^e\} = - \int_A N^T \left(\frac{\partial^2 \bar{\psi}}{\partial z^2} + r \frac{\partial}{\partial r} \left(\frac{1}{r} \frac{\partial \bar{\psi}}{\partial r} \right) - r Ra \frac{\partial \bar{T}}{\partial r} \right) dV \quad (2.3.1)$$

$$\{R^e\} = - \int_A N^T \left(\frac{\partial^2 \bar{\psi}}{\partial z^2} + r \frac{\partial}{\partial r} \left(\frac{1}{r} \frac{\partial \bar{\psi}}{\partial r} \right) - r Ra \frac{\partial \bar{T}}{\partial r} \right) 2\pi r dA \quad (2.3.2)$$

where R^e is the residue. Considering the individual terms of equation (2.3.2)

The differentiation of following term results into

$$\frac{\partial}{\partial r} \left([N^T] \frac{\partial \bar{\psi}}{\partial r} \right) = [N^T] \frac{\partial^2 \bar{\psi}}{\partial r^2} + \frac{\partial [N^T]}{\partial r} \frac{\partial \bar{\psi}}{\partial r} \quad (2.3.3)$$

Thus

$$\int_A N^T \frac{\partial^2 \bar{\psi}}{\partial r^2} dA = \int_A \frac{\partial}{\partial r} \left([N^T] \frac{\partial \bar{\psi}}{\partial r} \right) 2\pi r dA - \int_A \frac{\partial [N^T]}{\partial r} \frac{\partial \bar{\psi}}{\partial r} \quad (2.3.4)$$

The first term on right hand side of equation (2.3.4) can be transformed into surface integral by the application of Greens theorem and leads to inter-element requirement at boundaries of an element. The boundary conditions are incorporated in the force vector.

Let us consider that the variable to be determined in the triangular area as “T”.

The polynomial function for “T” can be expressed as

$$T = \alpha_1 + \alpha_2 r + \alpha_3 z \quad (2.3.5)$$

The variable T has the value T_i, T_j & T_k at the nodal position i, j & k of the element. The r and z co-ordinates at these points are r_i, r_j, r_k and z_i, z_j, z_k respectively.

$$\text{Since } T = N_i T_i + N_j T_j + N_k T_k \quad (2.3.6)$$

Where N_i, N_j & N_k are shape functions given by

$$N_m = \frac{a_m + b_m r + c_m z}{2A} \quad (2.3.7)$$

Making use of (2.3.7) give

$$\int_A N^T \frac{\partial^2 \bar{\psi}}{\partial r^2} 2\pi r dA = - \int_A \frac{\partial N^T}{\partial r} \frac{\partial N}{\partial r} \begin{bmatrix} \bar{\psi}_1 \\ \bar{\psi}_2 \\ \bar{\psi}_3 \end{bmatrix} dA \quad (2.3.8)$$

Substitution of (2.3.7) into (2.3.8) gives

$$\begin{aligned}
 &= \frac{1}{(2A)^2} \int_A \begin{bmatrix} b_1 \\ b_2 \\ b_3 \end{bmatrix} [b_1 b_2 b_3] \begin{bmatrix} \bar{\psi}_1 \\ \bar{\psi}_2 \\ \bar{\psi}_3 \end{bmatrix} 2\Pi \bar{r} dA \\
 &= -\frac{2\Pi R}{4A} \begin{bmatrix} b_1^2 & b_1 b_2 & b_1 b_3 \\ b_1 b_2 & b_2^2 & b_2 b_3 \\ b_1 b_3 & b_2 b_3 & b_3^2 \end{bmatrix} \begin{bmatrix} \bar{\psi}_1 \\ \bar{\psi}_2 \\ \bar{\psi}_3 \end{bmatrix} \tag{2.3.9}
 \end{aligned}$$

Similarly

$$\int_A N^T \frac{\partial^2 \bar{\psi}}{\partial z^2} 2\Pi \bar{r} dA = -\frac{2\Pi R}{4A} \begin{bmatrix} c_1^2 & c_1 c_2 & c_1 c_3 \\ c_1 c_2 & c_2^2 & c_2 c_3 \\ c_1 c_3 & c_2 c_3 & c_3^2 \end{bmatrix} \begin{bmatrix} \bar{\psi}_1 \\ \bar{\psi}_2 \\ \bar{\psi}_3 \end{bmatrix} \tag{2.3.10}$$

The third term of equation (2.3.2) gives

$$\int_A N^T \bar{r} R a \frac{\partial \bar{T}}{\partial r} 2\Pi \bar{r} dA = R a \int_A N^T \bar{r} \frac{\partial \bar{T}}{\partial r} 2\Pi \bar{r} dA \tag{2.3.11}$$

Since $M_1 = N_1, M_2 = N_2, M_3 = N_3$

Where M_1, M_2 and M_3 are the area ratios of the triangle and N_1, N_2 and N_3 are the shape functions.

Replacing the shape functions in the above equation (2.3.11) gives

$$\int_A N^T \bar{r} R a \frac{\partial \bar{T}}{\partial r} 2\Pi \bar{r} dA = \bar{r} R a \int_A \begin{bmatrix} M_1 \\ M_2 \\ M_3 \end{bmatrix} \frac{\partial(N)}{\partial r} \begin{bmatrix} \bar{T}_1 \\ \bar{T}_2 \\ \bar{T}_3 \end{bmatrix} 2\Pi \bar{r} dA \tag{2.3.12}$$

$$\begin{aligned}
 &= R a \frac{A}{3} \begin{bmatrix} 1 \\ 1 \\ 1 \end{bmatrix} \frac{2\Pi \bar{R}^2}{2A} [b_1 + b_2 + b_3] \begin{bmatrix} \bar{T}_1 \\ \bar{T}_2 \\ \bar{T}_3 \end{bmatrix} \\
 &= \frac{2\Pi \bar{R}^2 R a}{6} \left\{ \begin{bmatrix} b_1 \bar{T}_1 + b_2 \bar{T}_2 + b_3 \bar{T}_3 \\ b_1 \bar{T}_1 + b_2 \bar{T}_2 + b_3 \bar{T}_3 \\ b_1 \bar{T}_1 + b_2 \bar{T}_2 + b_3 \bar{T}_3 \end{bmatrix} \right\} \tag{2.3.13}
 \end{aligned}$$

Now the momentum equation (2.3.13) leads to

$$\frac{2\Pi \bar{R}}{4A} \left\{ \begin{bmatrix} b_1^2 & b_1 b_2 & b_1 b_3 \\ b_1 b_2 & b_2^2 & b_2 b_3 \\ b_1 b_3 & b_2 b_3 & b_3^2 \end{bmatrix} + \begin{bmatrix} c_1^2 & c_1 c_2 & c_1 c_3 \\ c_1 c_2 & c_2^2 & c_2 c_3 \\ c_1 c_3 & c_2 c_3 & c_3^2 \end{bmatrix} \right\} \begin{bmatrix} \bar{\psi}_1 \\ \bar{\psi}_2 \\ \bar{\psi}_3 \end{bmatrix} + \frac{2\Pi \bar{R}^2 R a}{6} \left\{ \begin{bmatrix} b_1 \bar{T}_1 + b_2 \bar{T}_2 + b_3 \bar{T}_3 \\ b_1 \bar{T}_1 + b_2 \bar{T}_2 + b_3 \bar{T}_3 \\ b_1 \bar{T}_1 + b_2 \bar{T}_2 + b_3 \bar{T}_3 \end{bmatrix} \right\} = 0 \tag{2.3.14}$$

Which is in the form of the stiffness matrix

$$[K_s] \{ \bar{\psi} \} = \{ f \}$$

Similarly application of Galerkin method to Energy equation (2.2.14) gives

$$\{ R^e \} = - \int_A N^T \left[\frac{1}{r} \left(\frac{\partial \bar{\psi}}{\partial r} \frac{\partial \bar{T}}{\partial z} - \frac{\partial \bar{\psi}}{\partial z} \frac{\partial \bar{T}}{\partial r} \right) - \left(\frac{1}{r} \frac{\partial}{\partial r} \left(\left(1 + \frac{4R_d}{3} \right) r \frac{\partial \bar{T}}{\partial r} + \frac{\partial^2 \bar{T}}{\partial z^2} \right) \right) \right] 2\Pi \bar{r} dA \tag{2.3.15}$$

Considering the terms individually of the above equation (2.3.15)

$$\int_A [N]^T \frac{\partial \bar{\psi}}{\partial z} \frac{\partial \bar{T}}{\partial r} 2\Pi dA = \int_A \begin{bmatrix} M_1 \\ M_2 \\ M_3 \end{bmatrix} \frac{\partial [N]}{\partial z} \{\bar{\psi}\} \frac{\partial [N]}{\partial r} \{\bar{T}\} 2\Pi r dA \tag{2.3.16}$$

$$= \frac{2\Pi A}{3} X \frac{1}{4A^2} [c_1 \bar{\psi}_1 + c_2 \bar{\psi}_2 + c_3 \bar{\psi}_3] [b_1, b_2, b_3] \begin{bmatrix} \bar{T}_1 \\ \bar{T}_2 \\ \bar{T}_3 \end{bmatrix}$$

$$= \frac{2\Pi}{12A} \begin{bmatrix} c_1 \bar{\psi}_1 + c_2 \bar{\psi}_2 + c_3 \bar{\psi}_3 \\ c_1 \bar{\psi}_1 + c_2 \bar{\psi}_2 + c_3 \bar{\psi}_3 \\ c_1 \bar{\psi}_1 + c_2 \bar{\psi}_2 + c_3 \bar{\psi}_3 \end{bmatrix} [b_1, b_2, b_3] \begin{bmatrix} \bar{T}_1 \\ \bar{T}_2 \\ \bar{T}_3 \end{bmatrix} \tag{2.3.17}$$

Following the same above procedure

$$\int_A [N]^T \frac{\partial \bar{\psi}}{\partial r} \frac{\partial \bar{T}}{\partial z} 2\Pi dA = \int_A \begin{bmatrix} M_1 \\ M_2 \\ M_3 \end{bmatrix} \frac{\partial [N]}{\partial r} \{\bar{\psi}\} \frac{\partial [N]}{\partial z} \{\bar{T}\} 2\Pi dA$$

$$\int_A N^T \frac{\partial \bar{\psi}}{\partial r} \frac{\partial \bar{T}}{\partial z} 2\Pi dA = \frac{2\Pi}{12A} \begin{bmatrix} b_1 \bar{\psi}_1 + b_2 \bar{\psi}_2 + b_3 \bar{\psi}_3 \\ b_1 \bar{\psi}_1 + b_2 \bar{\psi}_2 + b_3 \bar{\psi}_3 \\ b_1 \bar{\psi}_1 + b_2 \bar{\psi}_2 + b_3 \bar{\psi}_3 \end{bmatrix} [c_1, c_2, c_3] \begin{bmatrix} \bar{T}_1 \\ \bar{T}_2 \\ \bar{T}_3 \end{bmatrix} \tag{2.3.18}$$

The remaining two terms of energy equation can be evaluated in similar fashion of Momentum equation gives

$$\int_A N^T \left[\frac{1}{r} \frac{\partial}{\partial r} \left(\left\{ 1 + \frac{4}{3} R_d \right\} r \frac{\partial \bar{T}}{\partial r} \right) \right] 2\Pi r dA = - \left\{ 1 + \frac{4}{3} R_d \right\} \frac{2\Pi R}{4A} \begin{bmatrix} b_1^2 & b_1 b_2 & b_1 b_3 \\ b_1 b_2 & b_2^2 & b_2 b_3 \\ b_1 b_3 & b_2 b_3 & b_3^2 \end{bmatrix} \begin{bmatrix} \bar{T}_1 \\ \bar{T}_2 \\ \bar{T}_3 \end{bmatrix} \tag{2.3.19}$$

$$\int_A N^T \frac{\partial^2 \bar{T}}{\partial z^2} 2\Pi r dA = - \frac{2\Pi R}{4A} \begin{bmatrix} c_1^2 & c_1 c_2 & c_1 c_3 \\ c_1 c_2 & c_2^2 & c_2 c_3 \\ c_1 c_3 & c_2 c_3 & c_3^2 \end{bmatrix} \begin{bmatrix} \bar{T}_1 \\ \bar{T}_2 \\ \bar{T}_3 \end{bmatrix} \tag{2.3.20}$$

Thus the stiffness matrix of Energy equation (2.3.14) is given by:

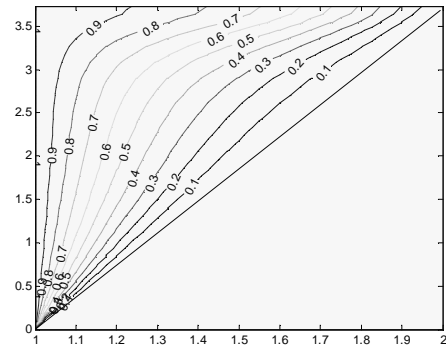
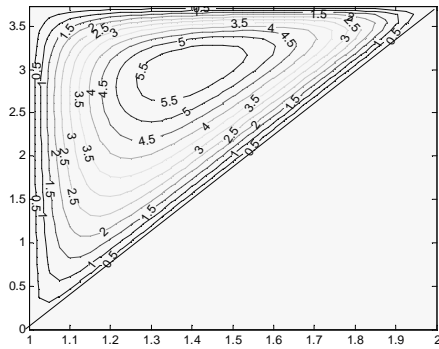
$$\left[\frac{2\Pi}{12A} \begin{bmatrix} c_1 \bar{\psi}_1 + c_2 \bar{\psi}_2 + c_3 \bar{\psi}_3 \\ c_1 \bar{\psi}_1 + c_2 \bar{\psi}_2 + c_3 \bar{\psi}_3 \\ c_1 \bar{\psi}_1 + c_2 \bar{\psi}_2 + c_3 \bar{\psi}_3 \end{bmatrix} [b_1, b_2, b_3] - \frac{2\Pi}{12A} \begin{bmatrix} b_1 \bar{\psi}_1 + b_2 \bar{\psi}_2 + b_3 \bar{\psi}_3 \\ b_1 \bar{\psi}_1 + b_2 \bar{\psi}_2 + b_3 \bar{\psi}_3 \\ b_1 \bar{\psi}_1 + b_2 \bar{\psi}_2 + b_3 \bar{\psi}_3 \end{bmatrix} [c_1, c_2, c_3] \right] \begin{bmatrix} \bar{T}_1 \\ \bar{T}_2 \\ \bar{T}_3 \end{bmatrix}$$

$$+ \frac{2\Pi R}{4A} \left\{ \left\{ 1 + \frac{4}{3} R_d \right\} \begin{bmatrix} b_1^2 & b_1 b_2 & b_1 b_3 \\ b_1 b_2 & b_2^2 & b_2 b_3 \\ b_1 b_3 & b_2 b_3 & b_3^2 \end{bmatrix} \begin{bmatrix} \bar{T}_1 \\ \bar{T}_2 \\ \bar{T}_3 \end{bmatrix} + \begin{bmatrix} c_1^2 & c_1 c_2 & c_1 c_3 \\ c_1 c_2 & c_2^2 & c_2 c_3 \\ c_1 c_3 & c_2 c_3 & c_3^2 \end{bmatrix} \begin{bmatrix} \bar{T}_1 \\ \bar{T}_2 \\ \bar{T}_3 \end{bmatrix} \right\} = 0 \tag{2.3.21}$$

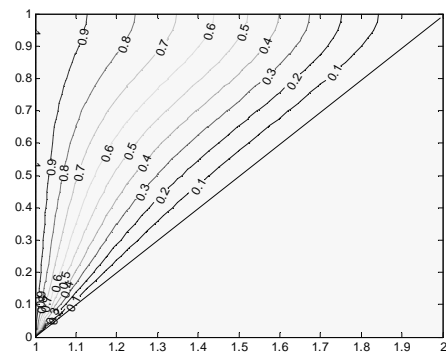
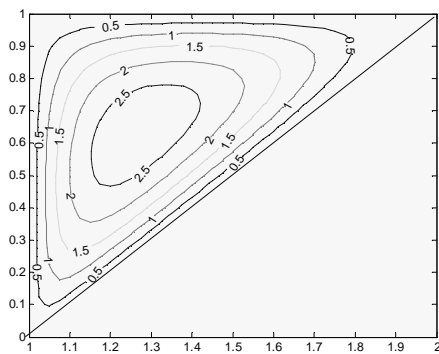
at $\bar{r} = \bar{r}_0$, $\bar{T} = 0$, $\bar{\psi} = 0$ (2.2.16)

RESULTS AND DISCUSSION

a)



b)



c)

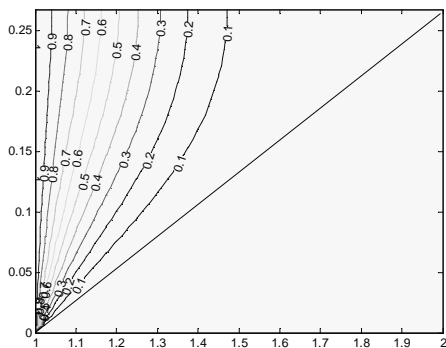
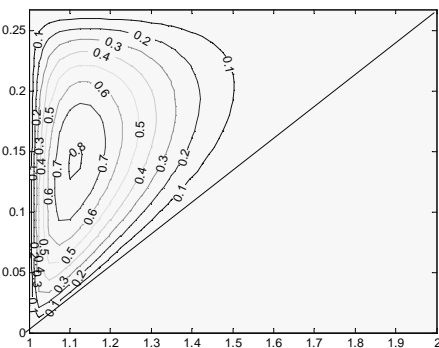
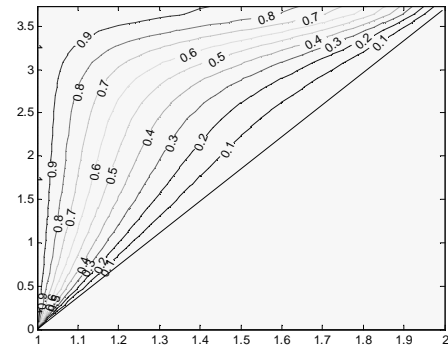
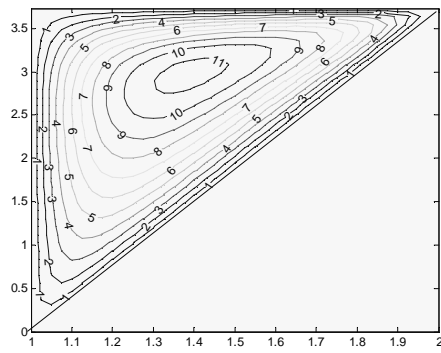
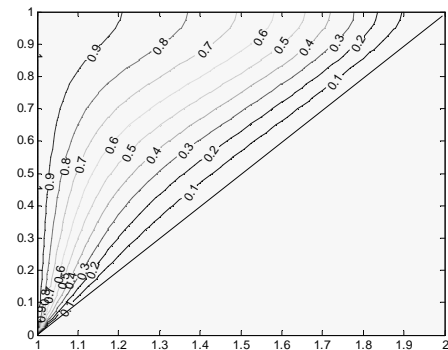
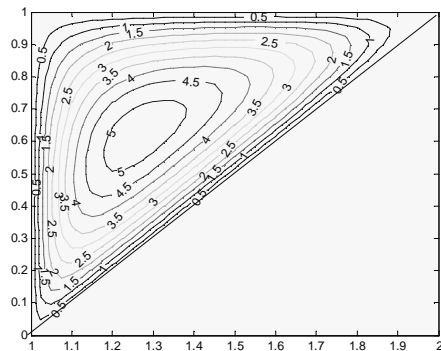


Fig: 2.4.1: Streamlines(left) and Isotherms(Right) for $Ra=50$, $R_r=1$, $R_d=1$
 a) $C_A=15$ b) $C_A=45$ c) $C_A=75$

a)



b)



c)

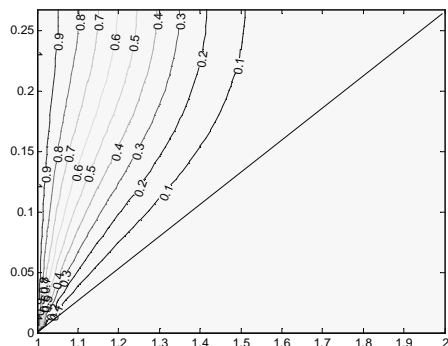
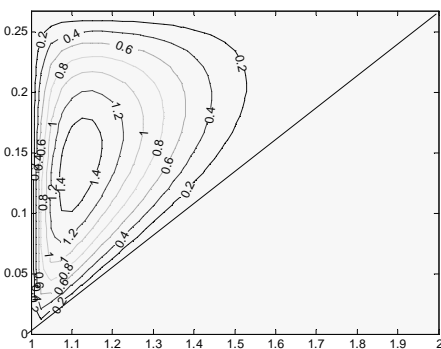


**Fig: 2.4.2: Streamlines(left) and Isotherms(Right) for $Ra=100$, $R_r=1$, $R_d=1$
a) $C_A=15$ b) $C_A=45$ c) $C_A=75$**

Fig (2.4.1.) shows the streamlines and isothermal lines inside porous medium for various values of Cone angle (C_A) at $Ra = 50$, $R_r = 1$ and $R_d = 1$. The fluid gets heated up near hot wall and moves up towards the cold wall due to high buoyancy force and then returns to hot wall of the vertical annular cone. The boundary layer thickness decrease with the increase of the Cone angle(C_A).

Fig (2.4.2) Shows the streamlines and isothermal lines distribution inside the porous medium for various values of Cone angle (C_A) at $Ra = 100$, $R_r = 1$, and $R_d = 1$. With increase of the Rayleigh number (Ra) the thickness of the boundary layer decreases relatively with the Fig (2.4.1) as expected.

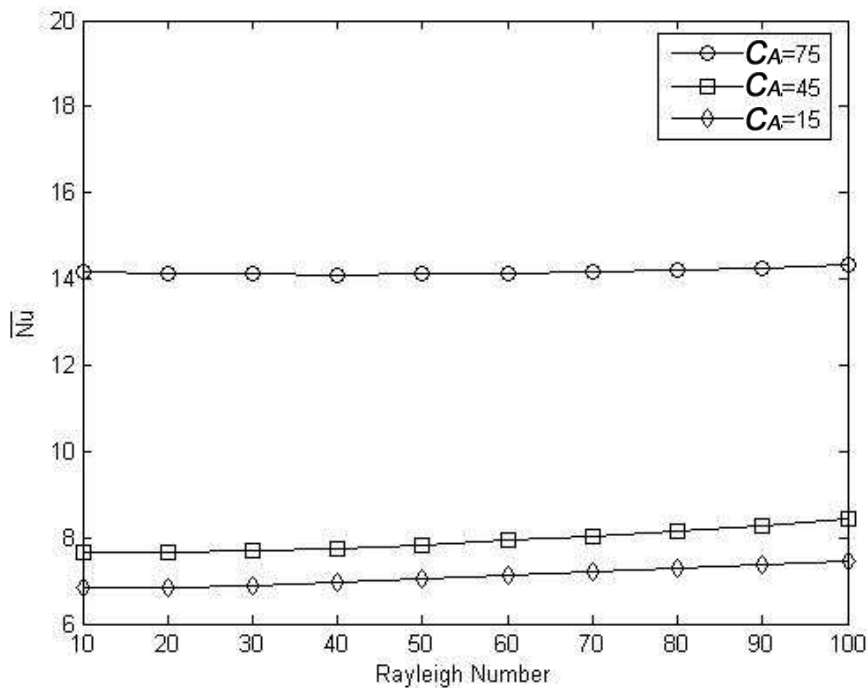


Fig. 2.4.3 : \bar{Nu} variations with Ra at hot surface for different values of C_A at $R_r=1, R_d=1$

Fig (2.4.3) shows the variation of average Nusselt number (\bar{Nu}) at hot wall, with respect to Rayleigh number (Ra) of the vertical annular cone for various values of Cone angle (C_A) at $R_r = 1, R_d = 1$. It is found that the average Nusselt number (\bar{Nu}) increases with increase in Rayleigh number (Ra). It can be seen that the average Nusselt number (\bar{Nu}) increases with increase in Cone angle (C_A) for a given Rayleigh number (Ra). The difference between the average Nusselt number at two different values of Cone angle (C_A) increases with Cone angle (C_A) for instance, the average Nusselt number (\bar{Nu}) increased by 11.4% when Cone angle (C_A) is increased from 15 to 45 $Ra = 10$. However the average Nusselt number (\bar{Nu}) increased by 13.8%, when Cone angle (C_A) is increased from 15 to 45 at $Ra = 100$. This difference becomes more prominent as the Rayleigh number (Ra) increases for particular value of Cone angle (C_A).

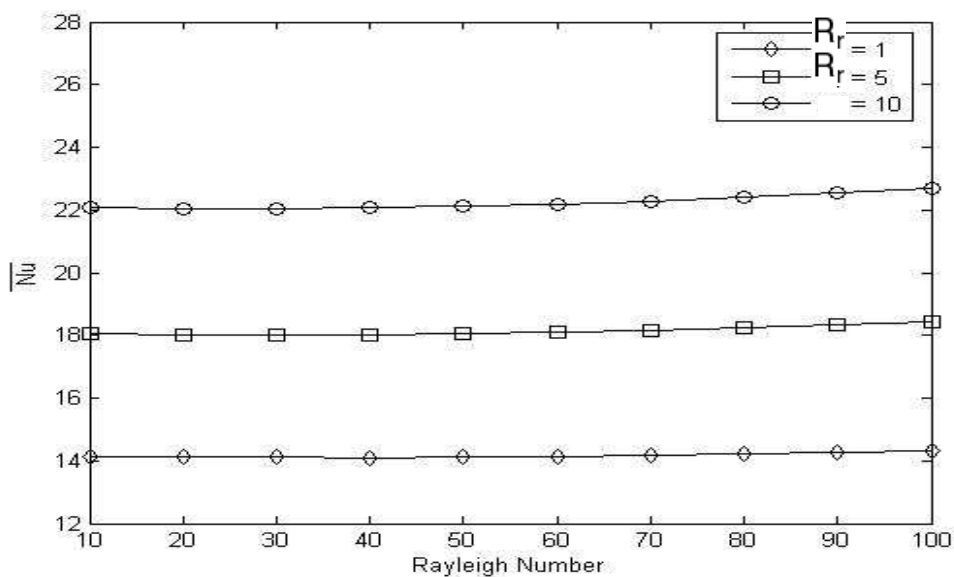


Fig.2.4.4: \bar{Nu} variations with Ra at hot surface for different values of R_r at $C_A=75, R_d=1$

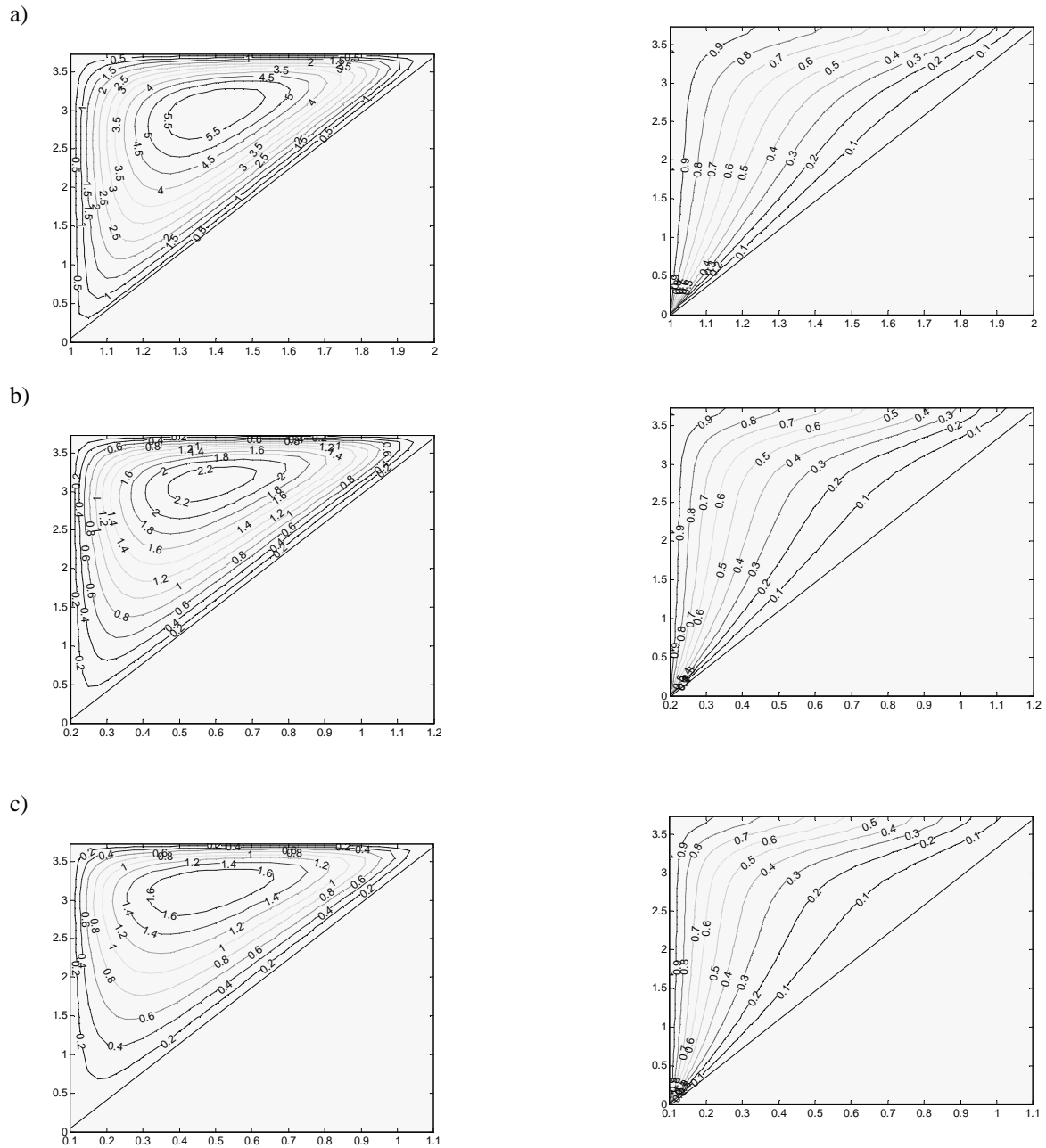


Fig: 2.4.5: Streamlines(left) and Isotherms(Right) for $Ra=50$, $C_A=15$, $R_d=1$
 a) $R_i=1$ b) $R_i=5$ c) $R_i=10$

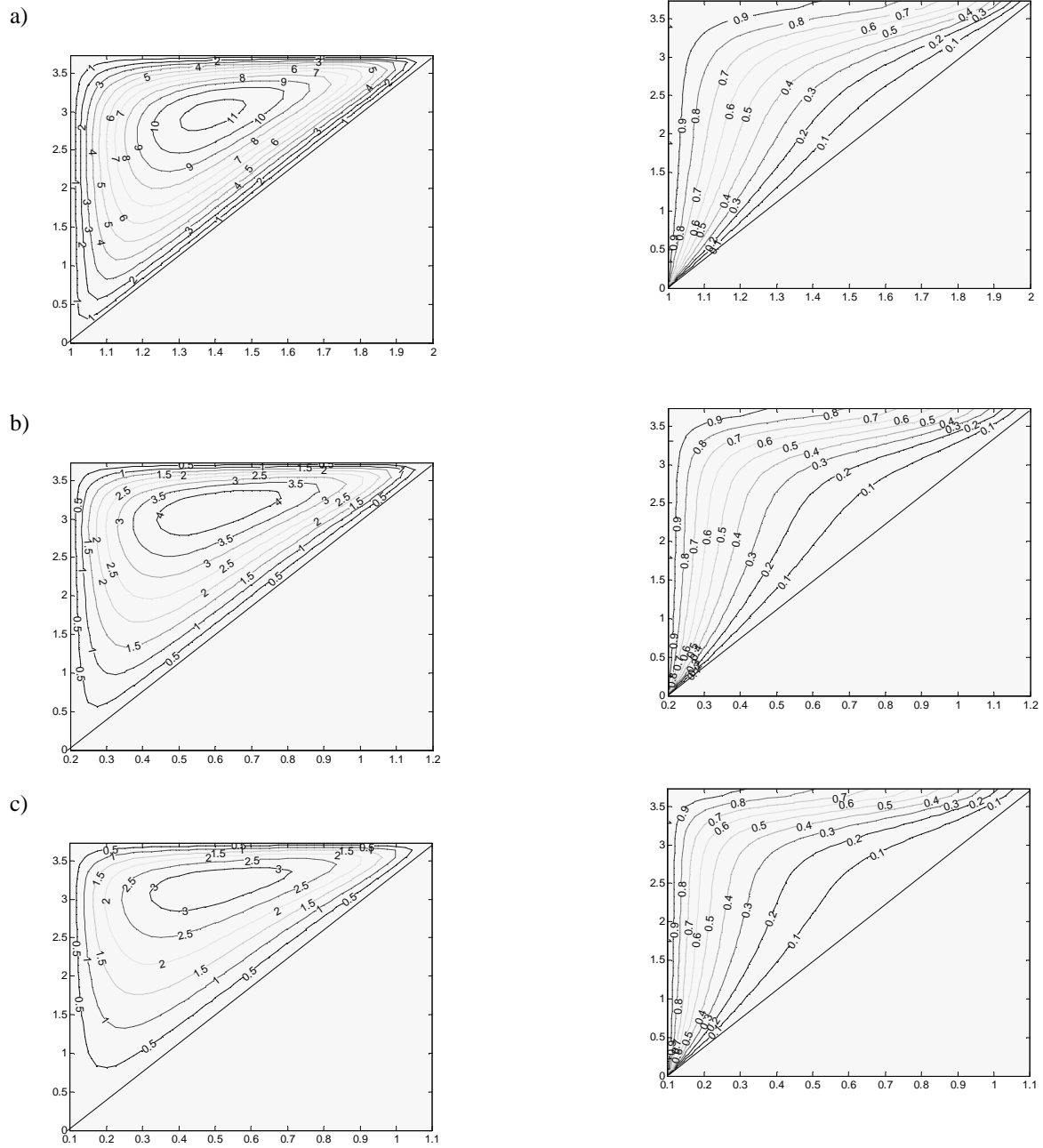


Fig:2.4.6: Streamlines(left) and Isotherms(Right) for $Ra=100$, $C_A=15$, $R_d=1$
 a) $R_i=1$ b) $R_i=5$ c) $R_i=10$

Fig (2.4.4) depicts the average Nusselt number (\bar{Nu}) at hot wall with respect to Rayleigh number (Ra), for various values of Radius ratio (R_r). This figure corresponds to the values $C_A = 75$, $R_d = 1$. It is found that the average Nusselt number (\bar{Nu}) increases with increase in Rayleigh number (Ra). It can be seen that the average Nusselt number (\bar{Nu}) increases with increase in Radius ratio (R_r). For a given Rayleigh number (Ra), the difference between the average Nusselt number at two different values of Radius ratio (R_r) increase with increase in Radius ratio (R_r). For instance, the average Nusselt number (\bar{Nu}) increased by 56%, when Radius ratio (R_r) is increased from 1 to 5 at $Ra=10$. However the average Nusselt number (\bar{Nu}) increased by 57% when Radius ratio (R_r) is increased from 1 to 5 at $Ra = 100$. This difference becomes more as the Rayleigh number (Ra) increases for particular value of Radius ratio (R_r).

Fig (2.4.5) shows the streamlines and isothermal lines inside the porous medium for various values of Radius ratio (R_r) at $Ra = 50$, $C_A = 15$ and $R_d = 1$. As the value of Radius ratio (R_r) increase the magnitude of the streamlines decreases. This is due to reason that the increased Radius ratio (R_r) promotes the fluid movement due to the higher buoyancy force, which in turn allows the convection heat transfer at lower portion of the hot wall of the vertical angular cone. The thermal boundary layer thickness decreases as the Radius ratio (R_r) increases.

Fig (2.4.6) Shows the streamlines and isothermal lines inside the porous medium for various values of Radius ratio (R_r) at $Ra = 100$, $C_A = 15$ and $R_d = 1$. With the comparison of the Fig (2.4.5) the boundary layer thickness of the Fig (2.4.6) decrease because of the increase of value of Rayleigh number ($Ra=100$).

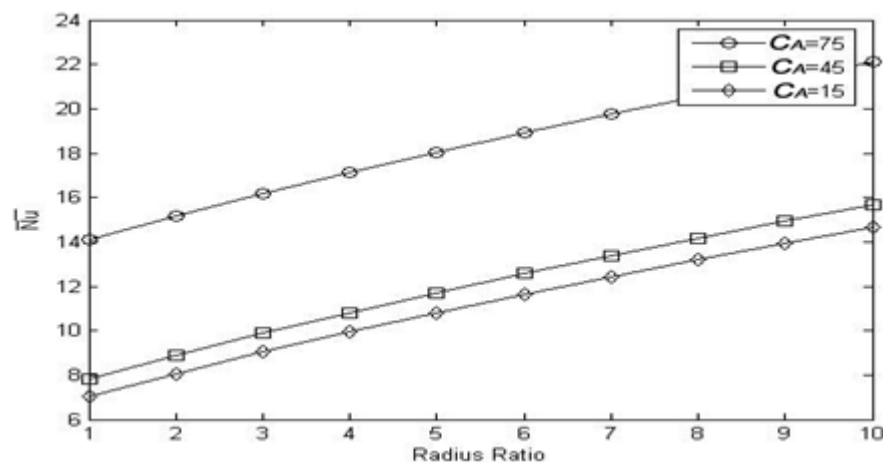
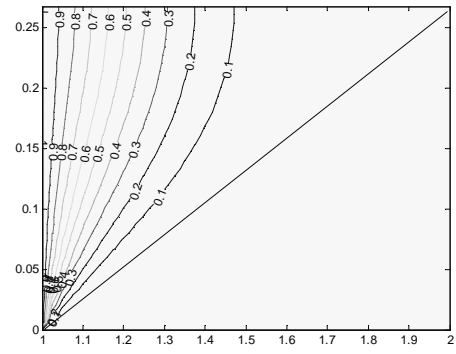
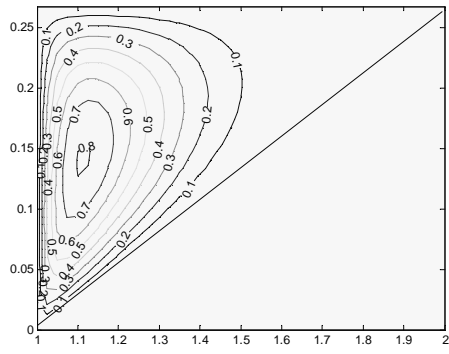


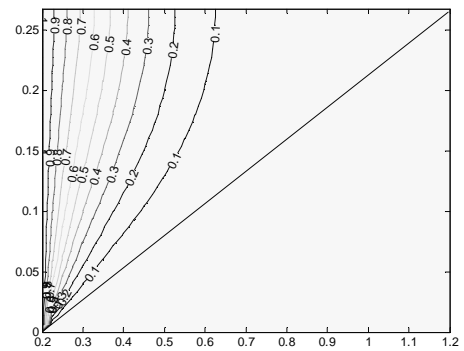
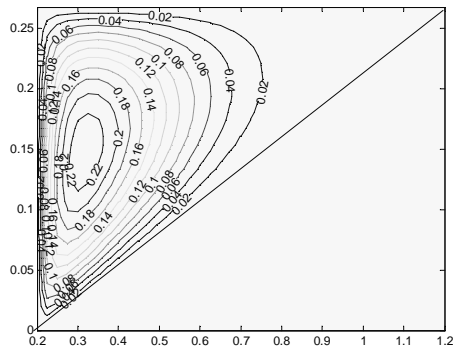
Fig.2.4.7: \bar{Nu} variations with R_r at hot surface for different values of C_A at $Ra=50$, $R_d=1$

Fig (2.4.7) illustrates the variation of average Nusselt number (\bar{Nu}) at hot wall, with respect to Radius ratio (R_r) of the vertical annular cone for various values of Cone angles (C_A) at values $Ra = 50$, $R_d = 1$. It is found that the average Nusselt number (\bar{Nu}) increases with increase in Radius ratio (R_r). It can be seen that the average Nusselt number (\bar{Nu}) increases with increase in Cone angle (C_A). For a given Radius ratio (R_r), the difference between the average Nusselt number (\bar{Nu}) for two difference values of Cone angle (C_A) increased with increase in Cone angle (C_A). For instance, the average Nusselt number (\bar{Nu}) increased 11.4%, when Cone angle (C_A) is increased 15 to 45, at $R_r = 1$. However the average Nusselt number (\bar{Nu}) increased 6.6% when cone angle is increased 15 to 45 at $R_r = 10$. This difference becomes more as the Radius ratio (R_r) increase.

a)



b)



c)

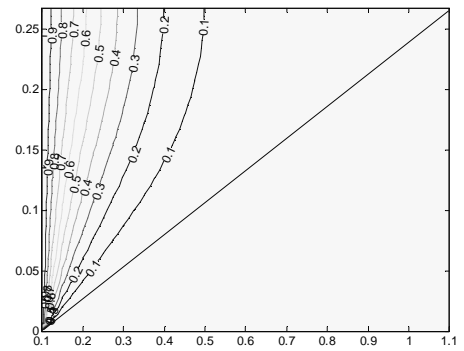
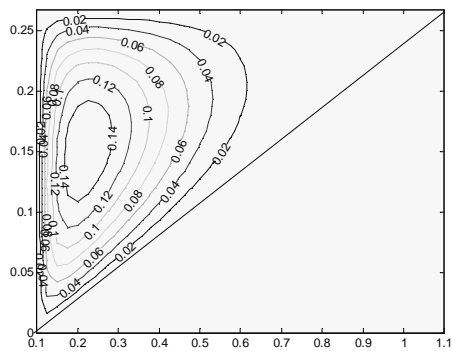


Fig:2.4.8: Streamlines(left) and Isotherms(Right) for Ra=50, CA=75, Ri=1
a) Ri=1 b) Ri=5 c) Ri=10

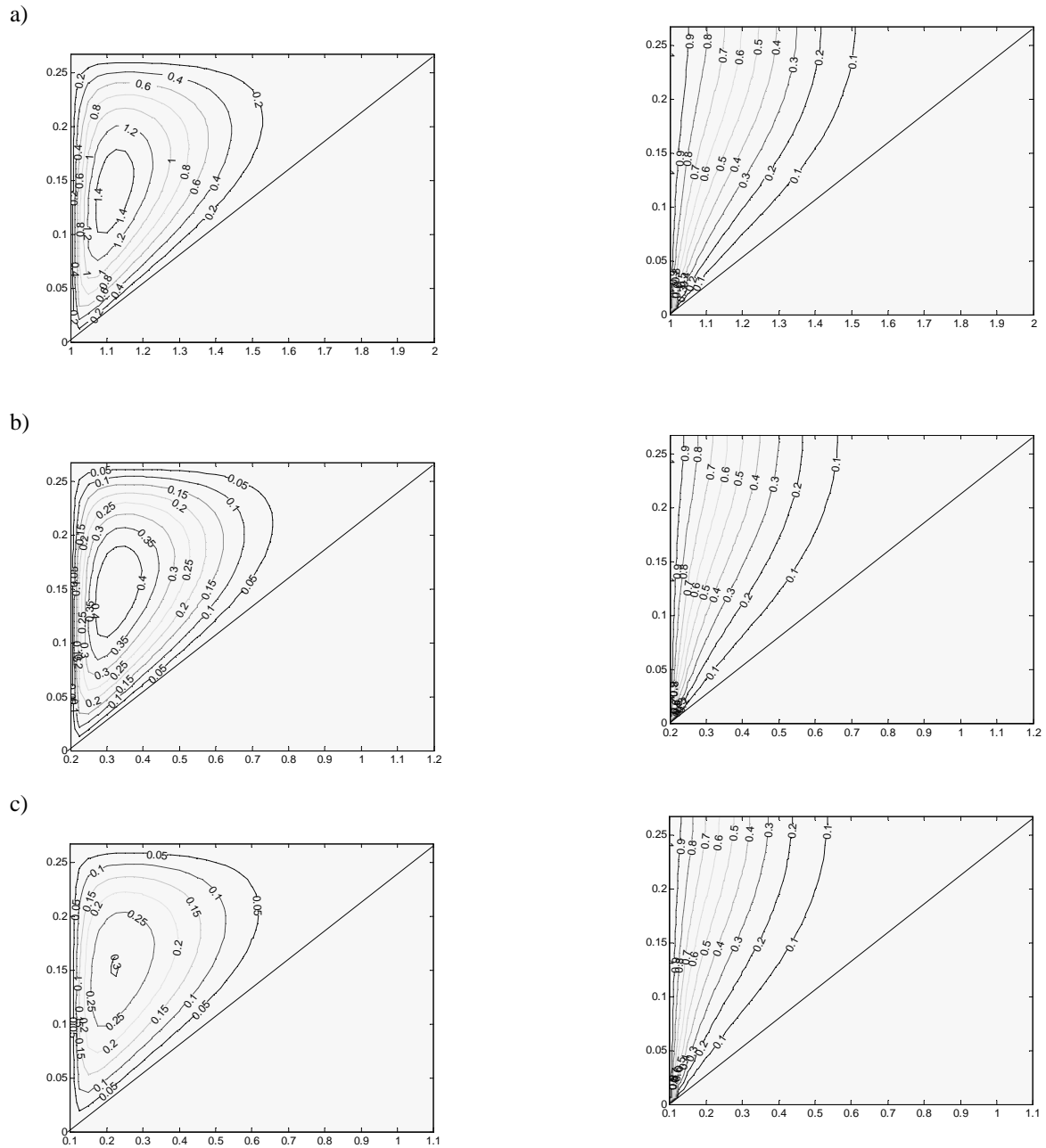


Fig:2.4.9: Streamlines(left) and Isotherms(Right) for Ra=100, CA=75, Rd=1
 a) Ri=1 b) Ri=5 c) Ri=10

Fig (2.4.8) represents the streamlines and isothermal lines for various values of Radius ratio (R_r) at $Ra = 50$, $C_A = 75$ and $R_d = 1$. It is clear from the streamlines and isothermal lines that the thermal boundary layer thickness decreases as the Radius ratio (R_r) increases. The magnitude of the streamlines increases as Radius ratio (R_r) increases and tends to move towards the cold wall of the vertical annular cone. At low Radius ratio (R_r) the streamlines tend to occupy the half domain of the vertical annular cone as compared to the higher value, of Radius ratio (R_r). It is clearly seen that more convection heat transfer take place as the upper portion of the vertical annular cone. The streamlines and isothermal lines shifts from the left upper portion of the hot wall to the upper portion of the cold wall of vertical annular cone as the Radius ratio (R_r) increases.

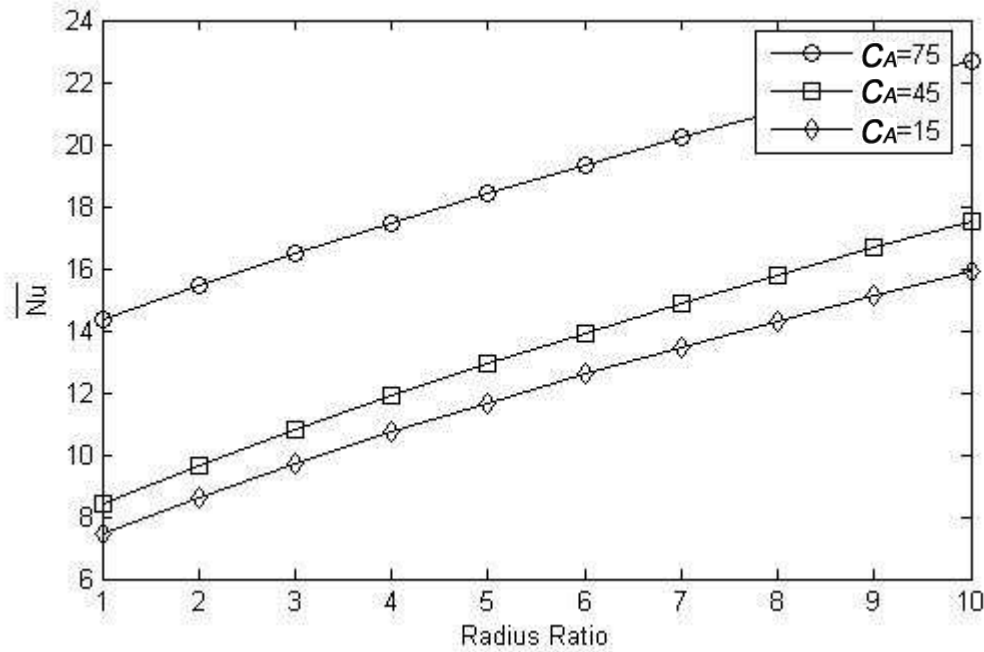


Fig.2.4.10: \overline{Nu} variations with R_r at hot surface for different values of C_A at $Ra=100$, $R_d=1$

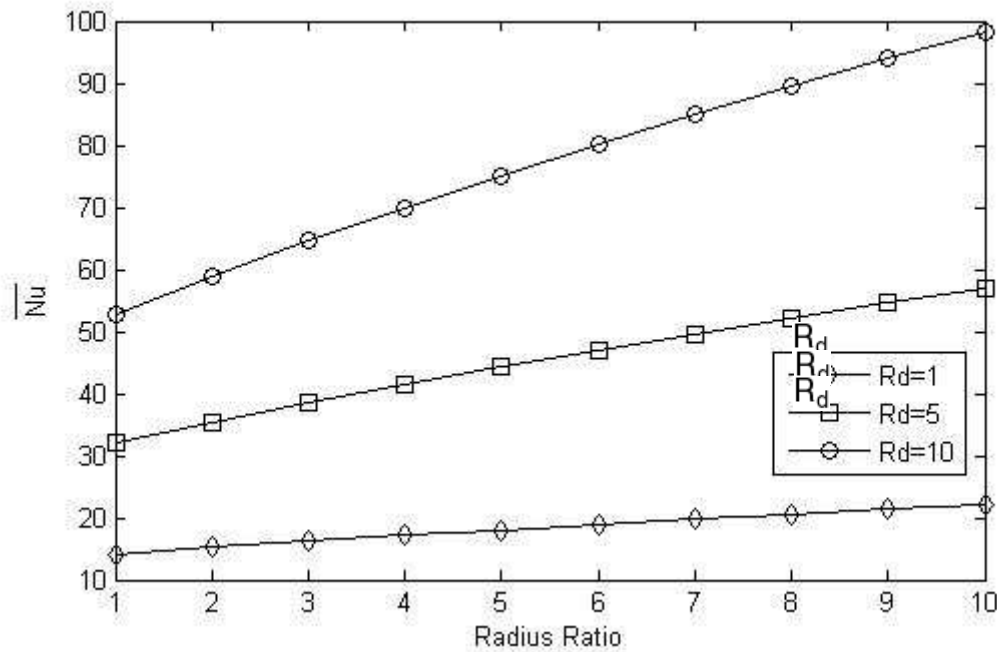


Fig.2.4.11: \overline{Nu} variations with R_r at hot surface for different values of R_d at $Ra= 50$, $C_A=75$

Fig (2.4.9) represents the streamlines and isothermal lines for various values of Radius ratio (R_r) at $Ra = 100$, $C_A = 75$ and $R_d = 1$. Almost connecting for Fig. 2.4.8 will hold good here also.

Fig (2.4.10) shows the variation of average Nusselt number (\bar{Nu}) at hot wall, with respect to Rayleigh number (Ra) of the vertical annular cone for various values of cone angle (C_A) at $Ra = 100$, $R_d = 1$. It is found that the average Nusselt number (\bar{Nu}) increases with increase in Radius ratio (R_r). It can be seen that the average Nusselt number (\bar{Nu}) increases with increase in Cone angle (C_A). For a given Radius ratio (R_r) the difference between the average Nusselt number (\bar{Nu}) at two different values of Cone angles (C_A) increases with increase in Cone angle (C_A). For instance, the average Nusselt number (\bar{Nu}) increases 11.8 %, when Cone angle (C_A) increased 15 to 45 at $R_r = 1$. However the average Nusselt number (\bar{Nu}) increased 6.2% when Cone angle (C_A) is increased 15 to 45 at $R_r = 10$. This difference becomes more prominent as the Radius ratio (R_r) increase. The average Nusselt number (\bar{Nu}) increases substantially when the Cone angle (C_A) increases for 45° to 75° .

Fig (2.4.11) depicts the average Nusselt number (\bar{Nu}) at hot wall with respect to Radius ratio (R_r), for various values of Radiation parameter (R_d). This figure corresponds to the values $Ra = 50$, $C_A = 75$. It is found that the average Nusselt number (\bar{Nu}) increases with increase in Radius ratio (R_r). It can also be seen that the average Nusselt number (\bar{Nu}) increases with increase in Radiation parameter (R_d). For a given Radius ratio (R_r), the difference between the average Nusselt number (\bar{Nu}) at two difference values of Radiation parameter (R_d) increases with increase in Radiation parameter (R_d). For instance the average Nusselt number (\bar{Nu}) increased by 128%, when Radiation parameter (R_d) is increased from 1 to 5, at $R_r = 1$. However the average Nusselt number (\bar{Nu}) increased by 159%, when Radiation parameter (R_d) is increased from 1 to 5, at $R_r = 10$. This difference becomes more prominent as the Radius ratio (R_r) increase.

REFERENCES

- [1] P.Cheng and W.J. Minkowycz, J, Geophysics, **1977**,82, 2040.
- [2] T.Y. Na and I. Pop, Int. J Engng Sci, **1983**, 21, 517.
- [3] RS.R.Gorla and A.H. Zinalabedini, ASME J. Energy Resources Technology, **1987** ,109, 26.
- [4] W.J. Minkowycz and P.Cheng, Int. J. Heat Mass Transfer, **1976**,19, 805.
- [5] A. Yücel, Numerical Heat Transfer, **1984**, 7, 483.
- [6] M. Kumari, I. Pop and G. Nath, Int. J. Heat Mass Transfer, **1985**,28, 2171
- [7] J.H. Merkin, acta mechanica, **1986**, 62, 19.
- [8] A.P. Bassom and D.A.S. Rees, Acta Mechanica,**1996** ,116, 139.
- [9] M.A. Hossain and I. Pop, Heat and Mass Transfer,**1997**,32,223.
- [10] A. Raptis, Int. comm. Heat Mass Transfer,**1998**, 25,289.
- [11]P. Cheng, Int. J. Heat Mass transfer,**1977**, 20, 893.
- [12] M.Kazmierczak, D. Poulikakos and I. Pop. Numerical Heat Transfer, **1986**, 10, 571
- [13] P. Cheng, Adv. Heat Transfer, **1979**,14, 1.
- [14]I.A. Hassanien, A.Y. Bakeir and R.S.R. Gorla, Heat and mass transfer, **1998**, 34, 209.
- [15] R.Viskanta and R.J. Grosh, Int, J. Heat and Mass Transfer, **1962**, 5, 795.
- [16] M.A. Ali, T.S. Chen and B.F. Armaly, AIAA J, **1984**, 22, 1797.
- [17] A.Y. Bakier, and R.S.R Gorla, Transport in porous media,**1996**, 23, 357 .
- [18] M.A. Hassain and D.A.S. Ress, Acta Mechanica, **1998** ,127, 63
- [19] A.Y. Baker, Int. comm. Heat mass Transfer,**2001**,28,119.
- [20] Srinadh, Advances in Applied Science Research, **2011**, 2 (6):215-222
- [21] J, Girish kumar, Advances in Applied Science Research, **2012**, 3 (4):2134-2140
- [22] K. Chand, Advances in Applied Science Research, **2012**, 3 (4):2169-2178
- [23] jyoti prakash, Advances in Applied Science Research, **2012**, 3 (4):2346-2354
- [24] Sravan N. Gaikwad, Advances in Applied Science Research, **2012**, 3 (3):1426-1434